Hillslope Evolution by Bedrock Landslides

Science
AAAS

2D sheet geometry.

From the calculated current stream function $F(x, y)$ in Fig. 3C, we can obtain the distribution of local sheet critical current densities $J_c(\mathbf{r}) = [(\partial F/\partial x)^2 + (\partial F/\partial y)^2]^{1/2}$ (Fig. 3D). The values are highly nonuniform, ranging from 10^5 to 10^6 A/cm² on a length scale at least 10 times as large as the average grain size. The percolative nature of the current is clear, as is the high suppression of J_c within the colony boundaries. These boundaries themselves are quite nonuniform and exhibit noticeable variations in J_c across the bridge on the scale of tens of micrometers. An extended low-J_c region meanders along the center of the bridge, where current loops on a scale of many grain sizes tend to form. The local $J_c(\mathbf{r})$ values in Fig. 3D correspond to intergranular, not intragranular, currents because the characteristic length scale of 50 to 100 μm over which J_c changes is much larger than the 5- to 10-μm Tl-1223 grain size. Analogous results were obtained from images taken for other temperatures between 9 and 77 K. For instance, the local $J_c(\mathbf{r})$ at 77 K and 24 mT could exceed 2×10^5 A/cm², although the transport J_c of the bridge at 77 K and 0 T was reduced to 1.9×10^4 A/cm² by three colony boundaries.

REFERENCES AND NOTES

1. D. H. Kim et al., Physica C **177**, 431 (1991).
2. E. D. Specht et al., ibid. **242**, 164 (1995).
3. Y. Iijima, N. Tanabe, O. Kohno, Y. Ikeno, Appl. Phys. Lett. **60**, 769 (1992); X. D. Wu et al., ibid. **67**, 2397 (1995).
4. D. C. Larbalestier et al., in Applied Superconductivity 1995 (Institute of Physics Conference Series Number 148, Institute of Physics, Philadelphia, 1995), vol. 1, pp. 29–34.
5. G. Blatter, M. V. Feigel'man, V. B. Geshkenbein, A. I. Larkin, V. M. Vinokur, Rev. Mod. Phys. **66**, 1125 (1994); E. H. Brandt, Rep. Prog. Phys. **58**, 1465 (1995); D. J. Bishop, P. L. Gammel, D. A. Huse, C. A. Murray, Science **255**, 165 (1992); H. Dai, S. Yoon, J. Liu, R. C. Budhani, C. M. Lieber, ibid. **265**, 1552 (1994).
6. D. Dimos, P. Chaudhari, J. Mannhart, Phys. Rev. B **41**, 4038 (1990); N. Heinig et al., Appl. Phys. Lett. **69**, 577 (1996).
7. A. Polyanskii et al., Phys. Rev. B **53**, 8687 (1996).
8. J. A. Parrell, A. A. Polyanskii, A. E. Pashitski, D. C. Larbalestier, Supercond. Sci. Technol. **9**, 393 (1996).
9. D. C. Larbalestier, Proceedings of the 10th Anniversary HTS Workshop on Physics, Materials and Applications (World Scientific, Rivers Edge, NJ, 1996), p. 41.
10. L. A. Dorosinskii et al., Physica C **203**, 149 (1992); C. A. Duran et al., Nature **357**, 474 (1992); Th. Schuster, M. R. Koblischka, B. Ludescher, H. Kronmuller, J. Appl. Phys. **72**, 1478 (1992); N. Nakamura, G. D. Gu, K. Takamuku, M. Murakami, N. Koshizuka, Appl. Phys. Lett. **61**, 3044 (1992).
11. A. E. Pashitski, A. Polyanskii, A. Gurevich, J. A. Parrell, D. C. Larbalestier, Physica C **246**, 133 (1995); Appl. Phys. Lett. **67**, 2720 (1995); U. Welp et al., Nature **376**, 44 (1995); Appl. Phys. Lett. **66**, 1271 (1995).
12. M. Turchinskaya et al., Physica C **216**, 205 (1993).
13. J. A. DeLuca et al., ibid. **205**, 21 (1993).
14. E. D. Specht et al., ibid. **226**, 76 (1994).
15. E. H. Brandt, Phys. Rev. B **46**, 8628 (1992).
16. B. J. Roth, N. G. Sepulveda, J. P. Wikswo Jr., J. Appl. Phys. **65**, 361 (1989).
17. P. D. Grant et al., Physica C **229**, 289 (1994); W. Xing, B. Heinrich, H. Zhou, A. A. Fife, A. R. Cragg, J. Appl. Phys. **76**, 4244 (1994); H. Niculescu, A. Saenz, M. Khankhasayev, P. J. Gielisse, Physica C **261**, 12 (1996).
18. Reconstruction of 2D current flow patterns in thin films from MO images. The sheet current $\mathbf{J}(\mathbf{r})$ in thin films can be expressed by the stream function $F(x, y)$

$$J_x(x,y) = \frac{\partial F}{\partial y}, \ J_y(x, y) = -\frac{\partial F}{\partial x} \quad (1)$$

The Fourier components $F(\mathbf{k})$ and $H_z(\mathbf{k})$ are related by the Biot-Savart law

$$H_z(k) = \frac{k}{2} e^{-k|z|} F(k) \quad (2)$$

where $k = |\mathbf{k}|$. For $z = 0$, the inverse Fourier transform of Eq. 2 yields

$$F(x, y) = \frac{1}{\pi} \int_{-\infty}^{\infty} \int_{-\infty}^{\infty} \frac{H_z(x',y')dx'dy'}{[(x - x')^2 + (y - y')^2]^{1/2}} \quad (3)$$

Equations 1 and 3 in principle enable the local current to be reconstructed from $H_z(x, y)$, obtained from the MO image. However, Eq. 3 requires integration of $H_z(x, y)$ over an infinitely large region, and $H_z(x, y)$ can only be measured in a finite domain, limited by the size of the MO film, the microscope field of view, and so forth. Moreover, the MO signal is measured at a nonzero distance $z_0 \sim 5$ μm above the surface, and $H_z(x, y)$ inevitably contains short-wavelength noise on a scale less than z_0 as a result of imperfections in the MO film. Because this noise produces fictitious "currents" in Eqs. 1 and 3, we used a noise reduction procedure (15), interpolating the digitized image signal by a spline and averaging it over a 6-μm by 6-μm grid. This suppresses irrelevant short-wave components of $H_z(x, y)$ by 7 to 10 times, without interfering with the larger scale variations of $H_z(x, y)$ caused by local inhomogeneities of $J_c(x, y)$. To avoid the restriction created by the finite area of $H_z(x, y)$ measurements, we rewrite Eq. 3 in the form

$$F(x, y) = \frac{1}{\pi} \int_{-b}^{b} dx' \int_{-a}^{a}$$
$$\times \frac{[H_z(x',y') - H_0(y')]dy'}{[(x - x')^2 + (y - y')^2 + \ell^2]^{1/2}} + F_0(y) \quad (4)$$

where $H_0(y)$ is the magnetic field that corresponds to the stream function $F_0(y)$, and the x axis is directed along the bridge. For infinite integration limits, Eq. 4 reduces to Eq. 3 for any $F_0(y)$. Now we choose $H_0(y)$ such that the main contribution to the integral in Eq. 4 comes from a $2b$ by $2a$ rectangle that includes the region of the bridge $|x| < 2w$, $|y| < w$, where $\mathbf{J}(\mathbf{r})$ was reconstructed ($2w$ is the bridge width). This can be done by taking $H_0(y)$, which gives the best fit to the measured $H_z(x, y)$ outside the sample ($|y| > w$), thus greatly improving the convergence of the integral in Eq. 4 and making it practically independent of a for $a > 2w$. We set $a = b = 4w$ and took $F_0(y)$ of the critical state model for a strip, for which $F_0(y) = J_{c0}(|y| - w)$ at $|y| \le w$, $F_0(y) = 0$ at $|y| > w$, and (7)

$$H_0 = \frac{J_{c0}}{\pi} \ln\left[\frac{(y^2 + z_0^2)^2}{(w^2 + y^2 + z_0^2)^2 - 4w^2 y^2} \right] + H_a \quad (5)$$

Here H_a is the applied field, and the averaged critical current density J_{c0} was determined by fitting the measured $H_z(x, y)$ with Eq. 5 beyond the bridge, $w < |y| < 4w$, where the influence of local inhomogeneities in the films is weak. For instance, a current loop of size L produces a field $H(r) \propto L/r^2$ at distance $r \gg L$, so the contribution to $H_z(\mathbf{r})$ from typical inhomogeneities with $L \approx 0.1w$ to $0.3w$ at $r = 2w$ to $3w$ is only a few percent of $H_z(\mathbf{r})$ at $r = L$. Notice that a, b, and $F_0(y)$ in Eq. 4 are only auxiliary quantities to account for the long-range character of $H_z(x, y)$ for the sheet geometry (19). We made sure that $\mathbf{J}(\mathbf{r})$ calculated from Eqs. 1 and 4 is indeed insensitive to the specific choice of $F_0(y)$. The value $\ell \sim z_0/2\pi$ in Eq. 4 accounts for $H_z(x, y)$ being measured at finite height z_0 and the fact that the Fourier components $F(k)$ with $k > 1/z_0$ should be excluded to avoid fictitious short-wavelength noise currents and thus to make the inversion scheme stable (16). We set $\ell = 0.8$ μm, but because ℓ is much smaller than the spatial resolution of our MO technique, the calculated $\mathbf{J}(\mathbf{r})$ only very weakly depends on ℓ.
19. E. H. Brandt and M. Indenbom, Phys. Rev. B **48**, 12893 (1993); E. Zeldov, J. R. Clem, M. McElfresh, M. Darwin, ibid. **49**, 9802 (1994).

Hillslope Evolution by Bedrock Landslides

Alexander L. Densmore,* Robert S. Anderson,
Brian G. McAdoo, Michael A. Ellis

Bedrock landsliding is a dominant geomorphic process in a number of high-relief landscapes, yet is neglected in landscape evolution models. A physical model of sliding in beans is presented, in which incremental lowering of one wall simulates baselevel fall and generates slides. Frequent small slides produce irregular hillslopes, on which steep toes and head scarps persist until being cleared by infrequent large slides. These steep segments are observed on hillslopes in high-relief landscapes and have been interpreted as evidence for increases in tectonic or climatic process rates. In certain cases, they may instead reflect normal hillslope evolution by landsliding.

Bedrock landsliding is an important process in the evolution of diverse landscapes (1–5). Most models of landscape evolution, however, assume that diffusive processes shape hillslopes (4, 6) or that slopes are instantaneously lowered above some threshold (7). Likewise, models of bedrock landslides have ignored long-term hillslope evolution by discrete events (8–11).

Several factors argue for the inclusion of discrete landslides in landscape evolution models. First, rates of landscape evolution

are dictated by both the magnitude and frequency distribution of geomorphic events (12). Also, as in other geomorphic systems (13), hillslope morphology depends on the sequence in which events have occurred. Hillslope profiles, and in particular steep hillslope toes, have been interpreted to reflect changes in channel incision rate, and thus in tectonic or climatic process rates (14). Finally, landslides can be a significantly nonsteady and nonuniform source of sediment to a fluvial system (2, 3).

We describe a model of hillslope evolution that involves perturbing a small pile of grains (15). Avalanche experiments have commonly been performed by slowly dropping grains onto the top of the pile (16), mimicking the special cases of taluses and dune slip faces. In our model, hillslopes are driven instead by the more common geomorphic mechanism of baselevel lowering (17).

Sand has been used in most physical models of avalanching, although Frette et al. (18) used rice to demonstrate the importance of grain shape anisotropy on avalanche dynamics and statistics. In most of our experiments, we used red beans, which are anisotropic (~1.9 cm by 0.8 cm by 0.6 cm) and tended to settle with their long axes horizontal, producing crude stratification of the model hillslope (19). The beans are analogous to blocks of rock whose strength is much higher than the strength of the boundaries between them. Thus, the beans approximate the behavior of a rock mass whose strength depends on both the shear strength of the zones of weakness within it and the anisotropy of the blocks. In the model, the strength of these planes did not change with time, although we expect that topographic stresses (10) and weathering should in time modify the strength and distribution of weakness planes in natural materials. In several of our experiments, we used white beans, which are less anisotropic (~1.0 cm by 0.6 cm by 0.5 cm) than are red beans. These tended to settle in a more random, less stratified configuration, similar to a sandpile or talus.

All model slides began at the toe of the hillslope, adjacent to the active boundary. Slides then propagated rapidly up the slope, so that a large volume of beans began to move almost simultaneously. Because slides never initiated away from the active boundary, the upper hillslope was only modified

by slides propagating from below. This stability allowed scarps and steep sections of hillslope to develop and persist. In addition, the shape anisotropy of the red beans resulted in the formation of coherent domains of grains that enabled the material to attain slopes of up to 90° (18).

The model had two phases of behavior during each run: a transient phase, during which the hillslope gradually lengthened toward the back wall of the model (Fig. 1A; profiles 0 through 5); and a steady phase, during which the hillslope maintained a constant horizontal length (Fig. 1A; profiles 6 through 10). The slide distribution data described below are restricted to the steady phase (20).

We differentiated between those slides that removed beans from the entire hillslope, which we term "slope-clearing events," and those that involved only part of the hillslope. Figure 1C shows a portion of the history of landslide sizes from a single experiment. Slope-clearing events (marked by dashed lines) occurred on average once every 3.6 ± 1.3 cm of boundary drop. They were separated from one another by smaller slides, and often by periods of no sliding (21). Slope-clearing events represented less than 10% of all slides (Fig. 2A), yet they accounted for 70% of the mass involved in sliding (Fig. 2B) (22).

Lowering the active boundary created a volume of unstable material above potential failure planes that emerged at the toe of the hillslope. This volume was an upper limit on potential slide size; it increased with

boundary drop and topographic slope, and it was reduced by any landslide that occurred. Large, slope-clearing events removed beans from the entire hillslope and thus smoothed the topography, although they did not necessarily leave behind a uniform slope. Profile 10 in Fig. 1A shows that the slope immediately following one slope-clearing event varied considerably about the mean slope (measured from the toe of the slope to the ridge crest) of 38°.

Because most model slides were relatively small (Fig. 2B), they affected only the area near the toe of the hillslope (22). This concentration of activity created a steep toe (Fig. 1A; especially profiles 5, 7, and 8). Larger slides, involving the lower one-half to two-thirds of the hillslope, left a head scarp just above their uppermost extent (Fig. 1A; especially profiles 7 through 9). Many steep toes and head scarps were underlain by coherent domains of closely packed beans.

In summary, the progression from stable hillslope, through formation of a steep lower segment, to slope-clearing event and resetting of the stable slope, repeated itself throughout the experiments. Most of the mass leaving the hillslope did so in large, infrequent, slope-clearing events. Smaller slides, restricted to the lower part of the hillslope, were responsible for most of the observed variations in morphology. Therefore, any random snapshot of a hillslope would most likely catch it between slope-clearing events, and the hillslope would likely have a highly nonuniform slope.

Slide behavior and hillslope morphology

Fig. 1. (**A**) Surface profiles from a red-bean experiment. Profiles were recorded every 5.0 cm of boundary drop. Higher numbers represent later profiles. (**B**) As in (A), but taken from a white-bean experiment. (**C**) Part of a time series of slide sizes from a red-bean experiment. Slope-clearing events are marked by the dashed vertical lines. Slide sizes are bimodally distributed, and most events are small (<100 g). (**D**) As in (C), but taken from a white-bean experiment. Peak slide sizes are smaller (note change in scale), and the distribution of sizes is more uniform. Slope-clearing events are both more frequent and smaller than in the red-bean experiments.
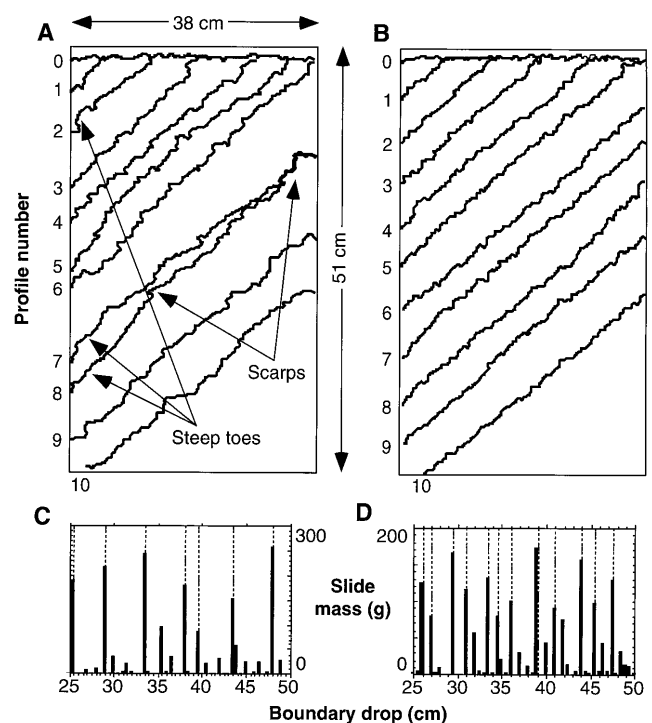
A. L. Densmore, R. S. Anderson, B. G. McAdoo, Institute of Tectonics and Department of Earth Sciences, University of California Santa Cruz, Santa Cruz, CA 95064, USA.
M. A. Ellis, Center for Earthquake Research and Information, University of Memphis, Memphis, TN 38152, USA.

*To whom correspondence should be addressed. E-mail: adens@earthsci.ucsc.edu

differed markedly between the red- and white-bean experiments. Coherent domains were absent in the white-bean experiments, and no scarps more than two grains high were observed. Hillslopes tended to be uniform; the steepest sections had slopes of at most a few degrees greater than the mean slope (Fig. 1B). Slope-clearing events were more frequent in white-bean experiments, occurring once per 2.1 ± 0.7 cm of boundary drop. Because less material was sequestered in steep segments, and less baselevel drop was available to accumulate unstable material, these slope-clearing events were on average smaller in the white-bean runs (Fig. 1D).

We suggest that the differences between red- and white-bean experiments were due to the differing shape anisotropy of red and white beans. The relation between slide size and the boundary drop since the last slide for the largest events was best described by a slip-predictable model (23). Failure depended on a trigger—in this case, the motion of the material at the toe of the hillslope (24). The size of the event was limited only by the amount of unstable material on the hillslope, which increased monotonically with boundary drop. Domains in the red beans formed knots that inhibited the propagation of smaller events (18). By contrast, hillslope toes in the white beans failed more readily,
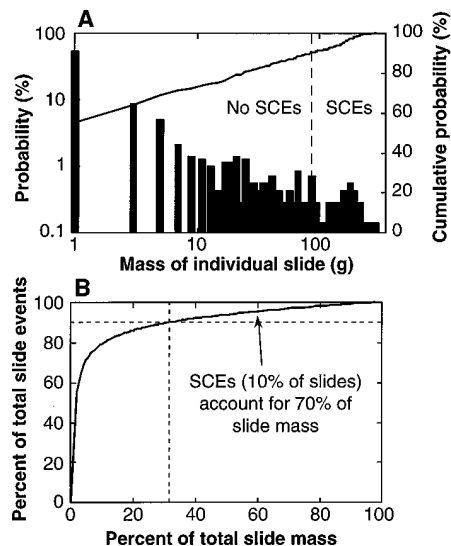
and the subsequent slide was more likely to be a slope-clearing event (25).

The geologic settings to which our model is most applicable are those in which the rock is highly fractured, and in which the

Fig. 3. (**A**) Hillslope profiles along the east bank of Redwood Creek, California, digitized from the Grouse Mountain, Lord-Ellis Summit, and Maple Creek U.S. Geological Survey 7.5′ topographic quadrangles. Vertical exaggeration is 2×. Profiles 1 through 3 show distinct inner gorges, whereas profile 4 is representative of more uniform slopes. (**B**) Illuminated perspective view of two submarine canyons cut into an anticline off the coast of central Oregon. Bathymetry data are from a multibeam survey of the fold-and-thrust belt near the toe of the Cascadia accretionary prism. Grid spacing is 75 m. Scale varies, but the thalwegs of canyons 1 and 2 are ~3 km apart. Maximum relief in canyons 1 and 2 is ~300 m and ~200 m, respectively. Letters A, B, and C mark the locations of the cross sections shown in Fig. 3C; arrows point to the endpoints of each section. (**C**) Profiles across canyons 1 and 2. Vertical exaggeration is 5×. The sections trend north-south, parallel to the strike of the anticline. Sections A and B show clearly defined inner gorges, 50 to 100 m deep.

strength of the rock mass is determined by the strength of the fractures (8) and the anisotropy of the blocks. We compared our observations with several examples of hillslopes in actively deforming regions.

Kelsey (3) described semicontinuous steep toes, or inner gorges (typically 50 to 200 m high) cut into schist and sandstone along Redwood Creek in northwestern California (Fig. 3A). In that area, hillslopes in competent sandstone (26) fail by episodic, bedrock-involved debris slides that are most common near the toe of the hillslope (2, 3), analogous to the bean model. Over a 2.5-year period, the largest 10% of landslides accounted for 60% of the total landslide volume (3). Kelsey (3) outlined conditions for the formation of an inner gorge, all of which are met by our model; they include the presence of a homogeneous rock type, continued downcutting at the slope base, and sufficient stream power to transport material away from the toe of the slope. He presented a conceptual model for inner gorge formation by parallel slope retreat (3), which is inconsistent with the transient inner gorges observed in our experiments.

A set of regularly spaced, headless submarine canyons have incised into an anticlinal ridge off the coast of central Oregon near the toe of the Cascadia accretionary prism (Fig. 3B). Steady-state in situ pore pressures are too low to induce sapping, and the steep canyon walls indicate that turbidity currents have periodically scoured the canyon floor (27). In cross section, several of the canyon walls show steep toes (Fig. 3C). A series of ALVIN dives revealed narrow slots on the floors of the canyons; the slots average 10 to 20 m high, 3 to 5 m wide, and several tens of meters long, and have vertical to overhanging walls. These observations suggest that bedrock landsliding is the primary process by which the canyon walls evolve. Turbidity currents incise the canyon floors, forming slot canyons and steep toes in the lower reaches of the canyons. Small landslides occur near the canyon floors, further defining the steep toes. Eventually, the canyon walls fail in major slope-clearing events (28).

The Indus River in northern Pakistan is incising into gneiss at rates of up to 12 mm/year in response to tectonic uplift of the Nanga Parbat-Haramosh massif (5). Bedrock walls in the Middle Gorge of the Indus may have slopes of up to 90° for several tens of meters above the river level, above which slopes are commonly ~32° (5). Large landslides have involved entire hillslopes, although they represent a small percentage of the drainage basin. Some tributaries have kept pace with the rapid incision of the Indus by excavating slot canyons with near-vertical walls up to 100 m high surmounted
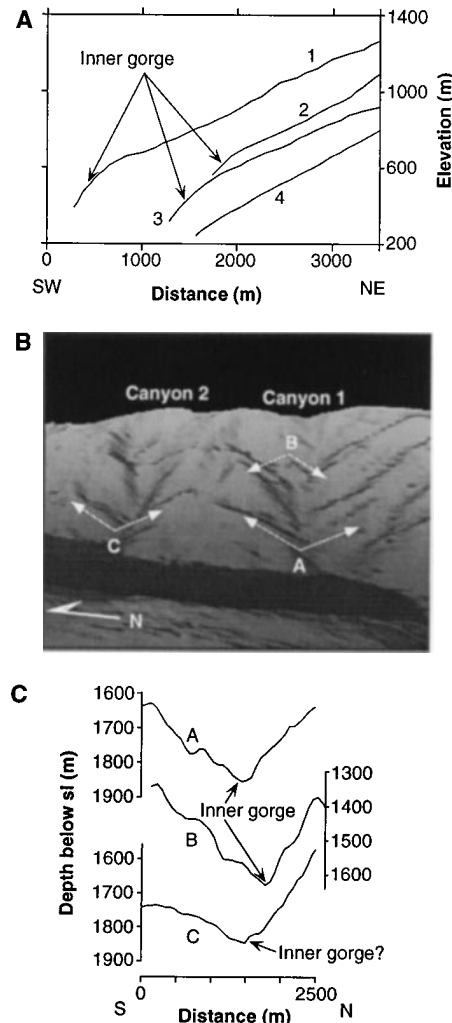

Fig. 2. (**A**) Probability distribution of model slides. Slides are from all red-bean experiments (*n* = 702) and are sorted into 2-g bins. Bars show the probability that a slide falls into a particular size bin. The solid curve shows the cumulative probability, in percent (note that scale is linear, rather than log). The vertical dashed line marks the smallest slope-clearing event (SCE). Slope-clearing events comprise 10% of the total number of slides. (**B**) Cumulative slide mass as a function of the total number of slides. The largest 10% of slides accounts for 70% of the total mass of beans involved in sliding.

by hillslopes that are much less steep.

In each of these examples, baselevel lowering has led to destabilization of the bounding hillslopes, resulting in steep toes that may coalesce along the channel to form inner gorges. Our experiments show that an inner gorge may well represent part of the natural development of hillslopes, rather than indicate tectonic or climatic rejuvenation. Because slope-clearing events are rare, instantaneous hillslope profiles will most likely show the steepened toes formed by smaller landslides. The detailed hillslope morphology, as well as the gross relief (11), may thus be a quantitative measure of the landscape-scale rock strength, at least in cases where this strength is controlled by discontinuities.

Hillslope profiles in the physical model are independent of the rate of boundary drop; no time scale is involved. We expect different system behavior if dynamic forces such as earthquakes are introduced, or if the strength of the rock mass is time dependent. If the rate of generation of low-strength fractures and joints is much higher than the rate of stripping, there will always be sufficient material of relatively low cohesion to yield deep-seated landslides, and we would expect hillslopes to evolve as in our experiments.

REFERENCES AND NOTES

1. M. L. Stout, *Geol. Soc. Am. Abstr. Programs* **16**, 257 (1984); P. C. Augustinus, *Earth Surf. Process. Land.* **17**, 39 (1992); J. M. Harbor, *Geol. Soc. Am. Bull.* **104**, 1364 (1992); S. W. Nelson, *U.S. Geol. Surv. Bull.* **2107**, 43 (1993); N. Hovius, C. P. Stark, P. A. Allen, *Geology*, in press.
2. H. M. Kelsey, *Geol. Soc. Am. Bull.* **91**, Part II, 1119 (1980).
3. _____, *Catena* **15**, 433 (1988).
4. R. S. Anderson, *J. Geophys. Res.* **99**, 20161 (1994).
5. D. W. Burbank *et al.*, *Nature* **379**, 505 (1996).
6. H. Kooi and C. Beaumont, *J. Geophys. Res.* **101**, 3361 (1996).
7. A. D. Howard, *Water Resour. Res.* **30**, 2261 (1994); G. E. Tucker and R. L. Slingerland, *J. Geophys. Res.* **99**, 12229 (1994).
8. K. Terzaghi, *Geotechnique* **12**, 251 (1962); M. J. Selby, *Z. Geomorphol.* **24**, 31 (1980).
9. M. J. Kirkby, in *Slope Stability: Geotechnical Engineering and Geomorphology*, M. G. Anderson and K. S. Richards, Eds. (Wiley, Chichester, UK, 1987), pp. 359–379.
10. D. J. Miller, thesis, University of Washington, Seattle (1993).
11. K. M. Schmidt and D. R. Montgomery, *Science* **270**, 617 (1995).
12. M. G. Wolman and J. P. Miller, *J. Geol.* **68**, 54 (1960).
13. A. B. Gibbons, J. D. Megeath, K. L. Pierce, *Geology* **12**, 327 (1984).
14. M. J. Selby, *Hillslope Materials and Processes* (Oxford Univ. Press, Oxford, 1993); J. R. Arrowsmith, D. D. Pollard, D. D. Rhodes, *J. Geophys. Res.* **101**, 6255 (1996).
15. The model consisted of two parallel, clear acrylic plates, each 51 cm by 38 cm by 0.6 cm thick. The 2.5-cm space separating the plates was filled with a granular material. Baselevel for the hillslope was determined by a sliding acrylic strip that formed one wall of the model (the active boundary), which was lowered at 0.5-cm intervals. Because all material reaching the toe of the hillslope was removed, no

buttressing of the hillslope was allowed. The mass of the removed material was measured on a digital balance with a precision of ±0.1 g.
16. See reviews in S. K. Grumbacher, K. M. McEwen, D. A. Halverson, D. T. Jacobs, J. Lindner, *Am. J. Phys.* **61**, 329 (1993); J. M. Carlson and G. H. Swindle, *Proc. Natl. Acad. Sci. U.S.A.* **92**, 6712 (1995).
17. This lowering could result from fluvial or glacial incision, by sea- or lake-level fall, or by dip-slip motion on a fault.
18. For example, V. Frette *et al.*, *Nature* **379**, 49 (1996).
19. We also evaluated the effect of structural dip on slide behavior [K. Terzaghi in (*8*); S. R. Hencher, in *Slope Stability: Geotechnical Engineering and Geomorphology*, M. G. Anderson and K. S. Richards, Eds. (Wiley, Chichester, UK, 1987), pp. 145–186] by creating horizontal stratigraphy and then tilting the entire model, either toward or away from the active boundary. This created either a dip-slope or antidip-slope, respectively.
20. The length of the hillslope imposed an upper bound on the size of a slide. By reporting only those results from the steady phase, we ensured that observed temporal variations in slide size were not due to changes in hillslope length.
21. J. Rosendahl, M. Vekic, J. Kelley, *Phys. Rev. E* **47**, 1401 (1993).
22. This agreed with observations of real hillslopes [W. F. Megahan, N. F. Day, T. M. Bliss, in *Forest Soils and Land Use; Proceedings of the Fifth North American Forest Soils Conference*, C. T. Youngberg, Ed. (Colorado State Univ., Ft. Collins, CO, 1978), pp. 116–139; (*2*)].
23. K. Shimazaki and T. Nakata, *Geophys. Res. Lett.* **7**, 279 (1980).
24. In contrast, time-predictable behavior would imply the existence of a threshold strength or steep toe height that must be exceeded before failure occurs. We saw no evidence for such a threshold.
25. Slides in the dip-slope experiments were smaller and more frequent than in the horizontal experiments for both red and white beans. We attributed this to the higher probability of favorably oriented failure planes in the dip-slope experiments [for example, Terzaghi (*8*)], which aided sliding and prevented large accumulations of material on the hillslope. By contrast, slides were much less frequent in the antidip-slope experiments because of the paucity of potential failure planes. Antidip-slope slides were also smaller than in the horizontal experiments, demonstrating the difficulty of removing material without favorably oriented failure planes.
26. S. M. Cashman, H. M. Kelsey, D. R. Harden, *U.S. Geol. Surv. Prof. Pap. 1454* (1995), pp. B1–B12.
27. B. G. McAdoo, D. L. Orange, E. Screaton, R. Kayen, H. Lee, *Am. Assoc. Pet. Geol. Bull.* **80**, 605 (1996).
28. L. F. Pratson and B. J. Coakley, *Geol. Soc. Am. Bull.* **108**, 225 (1996).
29. We thank D. Stakes of MBARI for access to her workstation and data visualization software; S. Anderson, G. Dick, K. Howard, and J. Repka for helpful discussions; H. Kelsey for observations and advice; and two anonymous reviewers for their comments. Supported by NASA Earth Systems Science graduate fellowship NGT-51220 to A.L.D. and by a grant from the NASA Surface Change Program. SeaBeam data collection and ALVIN dives were supported by Office of Naval Research grant N00014-9301-202.

22 August 1996; accepted 4 November 1996

An Explanation for Earth's Long-Term Rotational Stability

Mark A. Richards, Yannick Ricard, Carolina Lithgow-Bertelloni, Giorgio Spada, Roberto Sabadini

Paleomagnetic data show less than ~1000 kilometers of motion between the paleomagnetic and hotspot reference frames—that is, true polar wander—during the past 100 million years, which implies that Earth's rotation axis has been very stable. This long-term rotational stability can be explained by the slow rate of change in the large-scale pattern of plate tectonic motions during Cenozoic and late Mesozoic time, provided that subducted lithosphere is a major component of the mantle density heterogeneity generated by convection. Therefore, it is unnecessary to invoke other mechanisms, such as sluggish readjustment of the rotational bulge, to explain the observed low rate of true polar wander.

Movement of the Earth with respect to its axis of rotation on long time scales (10^3 to 10^9 years) is called polar wander, as distinguished from shorter term periodic or transient fluctuations, which are called wobble (*1*). Assuming that the average paleomagnetic axis corresponds to the paleorotation axis, paleomagnetic data can be used to measure the path of polar wander over continents or plates, which results mainly from plate tectonic motions. Paleomagnetic data can also be used to measure polar wander with respect to volcanic hotspots, such as Hawaii or Iceland, which appear to remain relatively fixed with respect to the more rapid global plate motions (*2*). This true polar wander (TPW) is generally taken as evidence that the mass redistribution resulting from mantle convection causes relative motion between Earth's principal inertia axis and the deep mantle source region for hotspots (*3*). Therefore, the paleomagnetic record of TPW provides a temporal constraint on

M. A. Richards, Department of Geology and Geophysics, University of California, Berkeley, CA 94720, USA.
Y. Ricard, Departement de Geologie, Ecole Normale Superieure, Lyon, France.
C. Lithgow-Bertelloni, Department of Terrestrial Magnetism, Carnegie Institution of Washington, Washington, DC 20015–1305, USA.
G. Spada, Dipartimento di Fisica, Settore Geofisica, Universita di Bologna, Bologna, Italy.
R. Sabadini, Dipartimento di Scienze della Terra, Sezione Geofisica, Universita di Milano, Milano, Italy.